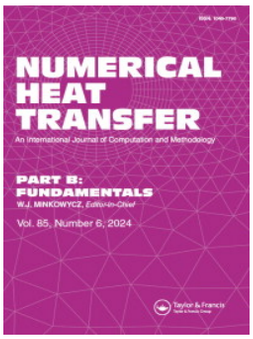

Taylor & Francis
Taylor & Francis Group

Numerical Heat Transfer, Part B: Fundamentals
An International Journal of Computation and Methodology

ISSN: (Print) (Online) Journal homepage: www.tandfonline.com/journals/unhb20

Geometric inverse estimation for the inner wall of a furnace under transient heat conduction based on dual reciprocity boundary element method

Bin Li, Xuejun Zhang & Xiangzhi Li

To cite this article: Bin Li, Xuejun Zhang & Xiangzhi Li (03 Oct 2023): Geometric inverse estimation for the inner wall of a furnace under transient heat conduction based on dual reciprocity boundary element method, Numerical Heat Transfer, Part B: Fundamentals, DOI: 10.1080/10407790.2023.2262744

To link to this article: https://doi.org/10.1080/10407790.2023.2262744

NUMERICAL HEAT TRANSFER, PART B: FUNDAMENTALS
https://doi.org/10.1080/10407790.2023.2262744

Geometric inverse estimation for the inner wall of a furnace under transient heat conduction based on dual reciprocity boundary element method

Bin Li[a,b], Xuejun Zhang[a,b], and Xiangzhi Li[a]

[a]Changchun Institute of Optics, Fine Mechanics and Physics, Chinese Academy of Sciences, Changchun, P.R. China; [b]University of Chinese Academy of Sciences, Beijing, P.R.China

ABSTRACT

A boundary shape estimation problem for the furnace's inner surface is solved using the dual reciprocity boundary element method (DRBEM) and the conjugate gradient method (CGM) under transient heat conduction. The DRBEM is utilized to eliminate the drawbacks of traditional numerical methods and classical boundary element method of discretizing the entire computational domain, with only boundary discretization. The inversion results are obtained by applying the CGM to minimize the objective function, in which the sensitivity coefficients are calculated with the complex variable derivation method (CVDM), making the calculation precise and independent of step size. To verify the accuracy of the DRBEM in solving the transient heat conduction problem, the influencing factors including radial-basis function, the number of internal collocation points, and time step size are investigated. The influences of measurement time interval, future time step, initial guess, measurement error, and the number and position of measurement points on the inversion results are analyzed. Meanwhile, the effectiveness of the proposed approach is tested by numerical examples, and the inversion results show that it is stable, accurate, and efficient for identifying different and complicated unknown boundary shapes of the furnace.

HIGHLIGHTS

- The boundary shape identification problem of the furnace wall is solved under transient heat conduction.
- The dual reciprocity boundary element method (DRBEM) is applied to solve the transient direct heat conduction problem, which retains the advantages of pure boundary discretization.
- In the conjugate gradient method (CGM), the sensitivity coefficients are calculated by the complex variable derivation method (CVDM) which is accurate and independent of the step size.
- The inner boundary shapes of the furnace with different complicated function forms are identified successfully.

ARTICLE HISTORY
Received 1 June 2023
Revised 23 August 2023
Accepted 18 September 2023

KEYWORDS
Complex variable derivation method; conjugate gradient method; dual reciprocity boundary element method; geometric inverse estimation; transient heat conduction

1. Introduction

Inverse heat conduction problems (IHCPs) are widely used in many engineering fields, including nuclear power, aerospace, and biological engineering. The IHCPs are often applied to estimate

CONTACT Bin Li libin_paper@163.com University of Chinese Academy of Sciences, Beijing 100049, P.R. China

Nomenclature

a	thermal diffusivity
$\boldsymbol{d}$	descent direction vector
f	approximate radial-basis function
$\boldsymbol{G}$, $\boldsymbol{H}$	geometry coefficient matric
J	objective function
L	number of inner collocation points
M	number of unknown geometric parameters
N	number of measurement points
N_b	number of boundary nodes
p	future time step
r	radius
$\boldsymbol{R}$	geometric parameter vector
t	time
T	temperature
$\boldsymbol{T}$	temperature vector
Δt	time step size
Δt_0	measurement time interval
$\hat{\boldsymbol{U}}$	coefficient matrices
$\boldsymbol{X}$	vector containing the unknown values
x, y	Cartesian coordinate system
W	the number of future time step

Greek Letters

α	search step size
β	conjugate coefficient
θ	polar angle
σ	standard deviation of the measurement error
ε	stopping criterion
ω	random number
Ω	computational domain
Γ	boundary of the domain Ω
$\boldsymbol{\phi}$	normal temperature gradient vector
$\boldsymbol{\phi}$	coefficient matrices

Subscripts

in	furnace inner boundary
out	furnace outer boundary

Abbreviations

BEM	boundary element method
DRBEM	dual reciprocity boundary element method
CGM	conjugate gradient method
CVDM	complex variable derivation method

boundary conditions [1–3], heat sources [4, 5], thermal properties [6–9], and geometry boundary shapes [10–14]. In many instances, the geometry boundary shape of a heat conduction problem is undetermined, and it can be estimated indirectly by measuring the temperature of some points located on the boundary or inside the domain. This is a typical IHCP for boundary shape identification, which is highly ill-posed due to the frequent change of geometry boundary during the inversion process [15], and is much more complicated than the other IHCPs.

During the operation of a furnace, the inner surface experiences extreme conditions of high temperature and high pressure, and is naturally damaged by corrosion and thermal stress. Therefore, it is critical to monitor the geometry shape and temperature of the inside boundary to guarantee the safety of the furnace. Many studies have been carried out to estimate the inner boundary shape or temperature of the furnace. Wang et al. [16] studied the inner boundary estimation problem of a furnace under steady-state heat conduction, while the direct problem was solved by the finite volume method (FVM). Chen et al. [17] identified the unknown inner boundary shape of a two-layer-wall furnace which is made of functionally graded materials. The FVM was applied to solve the direct problem of steady-state heat conduction. Su and Chen [18] estimated the inner boundary shape of the furnace under steady-state heat conduction, and the finite difference method (FDM) was utilized to solve the direct problem. Chen and Su [19] simultaneously estimated the temperature field of the outer boundary and the inner geometry boundary for a two-layer-wall furnace under steady-state heat conduction. The inversion solutions were obtained by means of the FDM, virtual area, and least-squares error method. Su et al. [20] solved the boundary identification problem of the furnace's inner surface under steady-state heat conduction using the FDM. Wang et al. [21] estimated the temperature distribution of the furnace's inside boundary under steady-state heat conduction using the FDM. Tan et al. [10] identified the boundary shape of the furnace's internal surface under steady heat conduction based on the meshless method. Yu et al. [22] estimated the unknown geometry boundary of the furnace based

on the concept of the virtual area and the boundary element method (BEM) under steady-state heat conduction. Yu et al. [23, 24] estimated the steady and unsteady boundary conditions of the furnace's inside boundary based on the BEM. Zhou et al. [25] adopted the finite element method (FEM) and the virtual boundary idea to identify the boundary shape under steady-state heat conduction.

On the one hand, it is worth pointing out that most references related to the inverse problem of a furnace apply the steady-state heat conduction condition to estimate the unknown boundary shape or boundary condition of a furnace. However, during the actual operation of a furnace, changes in thermal boundary conditions, such as temperature or heat flux are frequent and unavoidable. In many cases, it takes a long time to reach a steady state, which limits the application of inverse estimation based on steady-state heat conduction. As a result, it is of more practical significance to estimate the unknown boundary shape of a furnace under transient thermal boundary conditions.

On the other hand, traditional numerical methods, such as FDM, FEM, and FVM are mesh-based computing methods. During the inversion iteration process, these methods suffer from the repeated and tedious meshing of the entire computational domain, as well as mesh distortion in many situations. Many methods have been developed to overcome this shortcoming, including the least-squares collocation meshless method (LSCMM) [10], the method of fundamental solution (MFS) [26], the collocation Trefftz method [27], the boundary collocation method [28], the singular boundary method [29, 30], and the BEM [31]. The BEM discretizes the system boundary without mesh generation in the entire domain [32]. Previous applications of classical BEM in transient heat conduction have mostly used the time-dependent fundamental solution [33–35]. It requires to repeat calculating and saving the geometry-dependent influence coefficient matrices $\boldsymbol{H}$ and $\boldsymbol{G}$ at each time step, causing a significant increase in computational cost and memory consumption. In addition, the domain integral relating to the initial conditions needs to be calculated, which leads to the disappearance of the main advantage of the BEM, i.e. boundary-only integral. However, the dual reciprocity boundary element method (DRBEM) can eliminate this drawback by utilizing the fundamental solution of the Laplace equation [36], and this method has been widely applied in the transient IHCPs [36–38]. The DRBEM approximates the time derivative term with the concept of global interpolation and results in the boundary-only formulation. Thus, the DRBEM has obvious advantages in solving the transient IHCPs for boundary shape identification.

There are many optimization algorithms for solving inverse problems, such as the genetic algorithm [39], steepest descent method [40], Newton method [41], the least square method [42], Levenberg–Marquardt method [43], and conjugate gradient method (CGM) [10, 17, 44, 45]. Due to its effectiveness, accuracy, and stability, the CGM is one of the most popular optimization methods to solve almost all kinds of IHCPs, in which the calculation of sensitivity coefficients is the most important factor. Unlike the application of conventional FDM, the sensitivity coefficients can be determined using the complex variable derivation method (CVDM) which is accurate, fast, and independent of the step size [13, 46–50]. To the best of our knowledge, the applications of CVDM in CGM have rarely been reported.

In this study, the DRBEM and CGM are combined to estimate the unknown boundary shape of the furnace under transient heat conduction. During the inversion process of CGM, the CVDM is applied to calculate the sensitivity coefficients. The accuracy of DRBEM in solving the direct problem is examined by the influences of radial-basis function, the number of internal collocation points, and time step size. The proposed approach is compared with the conventional CGM in solving the inverse problem. To test the effectiveness of the proposed approach, the unknown boundary shapes with different and complex functional forms are considered, while the boundary conditions imposed on the unknown boundary also have different functional forms.

The effects of measurement time interval, future time step, initial guess, measurement error, and the number and position of measurement points on the estimation results are investigated.

2. The direct problem and DRBEM

A 2-D transient heat conduction problem of the furnace wall is shown in Figure 1. In this system, the radius of the outer boundary Γ_{out} is r_{out}, while the unknown radius of the inner boundary Γ_{in} is $r_{in}(\theta)$. Considering that the material properties are constant without an internal heat source or sink in the furnace wall domain Ω, the governing equation for the problem can be expressed as follows:

$$\frac{\partial^2 T(x,y,t)}{\partial x^2}+\frac{\partial^2 T(x,y,t)}{\partial y^2}=\frac{1}{a}\frac{\partial T(x,y,t)}{\partial t},\ (x,y)\in\Omega \text{ and } t\geq t_0 \tag{1}$$

where a is the thermal diffusivity, $T(x,y,t)$ is the temperature of point (x, y) at time t, and t_0 is the initial time.

The corresponding boundary conditions are stated as:

$$T(x,y,t)=T_{out},\quad (x,\ y)\in\Gamma_{out} \tag{2}$$

$$T(x,y,t)=T_{in}(x,y,t),\quad (x,\ y)\in\Gamma_{in} \tag{3}$$

where T_{out} is the constant temperature on boundary Γ_{out}, and $T_{in}(x,y,t)$ is the temperature on boundary Γ_{in} varying with the position (x, y) and time t.

The initial condition is given as:

$$T(x,y,0)=T_0(x,y) \tag{4}$$

where $T_0(x,y)$ is the initial temperature of the furnace wall.

The DRBEM adopts the fundamental solution of the Laplace equation, and the approximation of the time derivative term of Eq. (1) is expressed as: [51]

$$\frac{1}{a}\frac{\partial T(x,y,t)}{\partial t}\approx\sum_{j=1}^{N_b+L}\alpha_j(t)f_j(x,y) \tag{5}$$

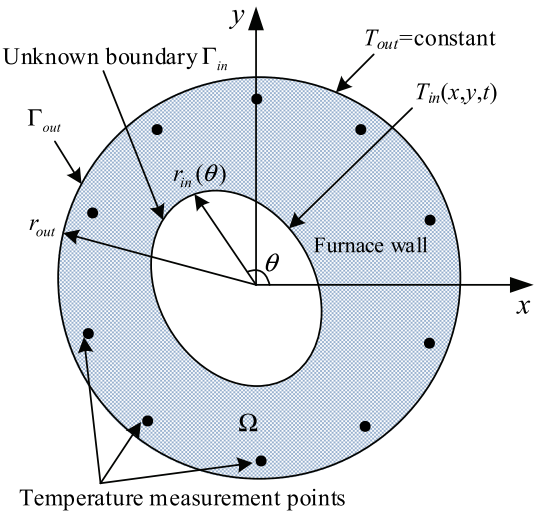

Figure 1. Diagram of the furnace wall for transient heat conduction problem.

where N_b denotes the node number on $\Gamma = \Gamma_{in} \cup \Gamma_{out}$, L denotes the collocation point number in domain Ω, $\alpha_j(t)$ is the time-dependent coefficient to be determined, and $f_j(x,y)$ is the approximate radial-basis function that satisfies the following equation:

$$f_j(x,y) = \nabla^2 \hat{u}_j(x,y) \tag{6}$$

Substituting Eqs. (5) and (6) into Eq. (1), the following equation can be obtained:

$$\frac{\partial^2 T(x,y,t)}{\partial x^2} + \frac{\partial^2 T(x,y,t)}{\partial y^2} \approx \sum_{j=1}^{N_b+L} \alpha_j(t) \nabla^2 \hat{u}_j(x,y) \tag{7}$$

Multiplying both sides of Eq. (7) by the fundamental solution $v(p,q)$ of the Laplace equation, integrating over the whole domain Ω, and using Green's second formula, the boundary integral equation as follows can be obtained:

$$\begin{aligned} c(p)T(p) + \int_\Gamma v(p,q)\phi(q)\mathrm{d}\Gamma_q - \int_\Gamma \phi^*(x,y)T(q)\mathrm{d}\Gamma_q \\ = \sum_{j=1}^{N_b+L} \alpha_j \left\{ c(p)\hat{u}_j(p) + \int_\Gamma v(p,q)\hat{\phi}(q)\mathrm{d}\Gamma_q - \int_\Gamma \phi^*(x,y)\hat{u}_j(q)\mathrm{d}\Gamma_q \right\} \end{aligned} \tag{8}$$

where

$$\phi(q) = \partial T(q)/\partial n_q \tag{9}$$

$$\phi^*(p,q) = \partial v(p,q)/\partial n_q \tag{10}$$

$$\hat{\phi}_j(q) = \partial \hat{u}_j(q)/\partial n_q \tag{11}$$

$$c(p) = \begin{cases} 1 & \text{for } p \text{ inside } \Omega \\ 0.5 & \text{for } p \text{ on the smooth boundary } \Gamma \\ 0 & \text{for } p \text{ outside } \Omega \end{cases} \tag{12}$$

$$v(p,q) = \frac{1}{2\pi} \ln \sqrt{(x_p - x_q)^2 + (y_p - y_q)^2} \tag{13}$$

Using the numerical calculation method, the boundary Γ is discretized into N_b boundary elements. In this study, we apply the constant element in which the curve boundary is approximated by a straight line, the node is in the midpoint of the straight line, and the values of the boundary temperature T and corresponding normal derivative $T_n = \partial T/\partial n$ over each element are equal to the constant values of the node. Applying Eq. (8) consecutively for N_b nodes , N_b equations are expressed in a matrix as:

$$\boldsymbol{HT} - \boldsymbol{G\phi} = (\boldsymbol{H\hat{U}} - \boldsymbol{G\hat{\phi}})\boldsymbol{\alpha} \tag{14}$$

where $\boldsymbol{H}$ and $\boldsymbol{G}$ are geometry-dependent influence coefficient matrices, $\boldsymbol{T}$ and $\boldsymbol{\phi}$ are, respectively, the temperature and corresponding normal gradient vectors for the boundary nodes, $\hat{\boldsymbol{U}}$ and $\hat{\boldsymbol{\phi}}$ are the coefficient matrices related to the radial basis function $f_j(x,y)$, and the vector $\boldsymbol{\alpha}$ contains the values of $\alpha_j(t)$ which can be determined through applying Eq. (5) to the boundary nodes and collocation points. The following expression can be obtained:

$$\frac{1}{a}\left\{\frac{\partial \boldsymbol{T}}{\partial t}\right\} = \boldsymbol{f\alpha} \tag{15}$$

where the square matrix $\boldsymbol{f}$ is defined as:

$$f_{ij} = f_j(x_i, y_i) \tag{16}$$

Then, the vector $\boldsymbol{\alpha}$ can be given by:

$$\boldsymbol{\alpha} = \frac{1}{a}\boldsymbol{f}^{-1}\left\{\frac{\partial \boldsymbol{T}}{\partial t}\right\} \tag{17}$$

Combining Eqs. (14) and (17), the following expression can be obtained:

$$\boldsymbol{HT} - \boldsymbol{G\phi} = \boldsymbol{C}\left\{\frac{\partial \boldsymbol{T}}{\partial t}\right\} \tag{18}$$

where the matric $\boldsymbol{C}$ is defined as:

$$\boldsymbol{C} = \frac{1}{a}(\boldsymbol{H}\hat{\boldsymbol{U}} - \boldsymbol{G}\hat{\boldsymbol{\phi}})\boldsymbol{f}^{-1} \tag{19}$$

Approximating the time derivative term by the FDM, Eq. (18) is rewritten as:

$$\boldsymbol{HT} - \boldsymbol{G\phi} = \boldsymbol{C}\frac{\boldsymbol{T}^{p+1} - \boldsymbol{T}^{p}}{\Delta t} \tag{20}$$

where p denotes the future time step, and Δt denotes the time step size.

Between the future time steps p and $p+1$, the difference parameters θ_t and θ_q are used for the vectors $\boldsymbol{T}$ and $\boldsymbol{\phi}$ in the form as follows:

$$\boldsymbol{T} = \theta_t \boldsymbol{T}^{p+1} + (1-\theta_t)\boldsymbol{T}^{p} \tag{21}$$

$$\boldsymbol{\phi} = \theta_q \boldsymbol{\phi}^{p+1} + (1-\theta_q)\boldsymbol{\phi}^{p} \tag{22}$$

Substituting Eqs. (21) and (22) into Eq. (20), the following expression can be derived: [51–54]

$$(\Delta t\theta_t \boldsymbol{H} - \boldsymbol{C})\boldsymbol{T}^{p+1} - (\Delta t\theta_q \boldsymbol{G})\boldsymbol{\phi}^{p+1} = [\Delta t(\theta_t - 1)\boldsymbol{H} - \boldsymbol{C}]\boldsymbol{T}^{p} - \Delta t(\theta_q - 1)\boldsymbol{G\phi}^{p} \tag{23}$$

where the parameters θ_t and θ_q usually take a value between 0.5 and 1. Due to its simplicity and adequate accuracy [13, 49, 50, 52–54], the purely backward time stepping method (i.e. θ_t=θ_q=1) is applied, and Eq. (23) can be rewritten as:

$$\left[\boldsymbol{H} - \frac{1}{\Delta t}\boldsymbol{C}\right]\boldsymbol{T}^{p+1} - \boldsymbol{G\phi}^{p+1} = -\frac{1}{\Delta t}\boldsymbol{C}\boldsymbol{T}^{p} \tag{24}$$

The right side of Eq. (24) is known from the future time step p or the initial condition. Introducing the boundary conditions of Eqs. (2) and (3) at the future time step $p+1$, carrying out the multiplication operation of the left side of Eq. (24), and moving all the unknowns and knowns to the left and right sides of the equation, respectively, then the equation can be rearranged to be:

$$\boldsymbol{A} \cdot \boldsymbol{X}^{p+1} = \boldsymbol{B}^{p+1} \tag{25}$$

where $\boldsymbol{A}$ is the square matrix containing the columns corresponding to the unknown boundary conditions at the future time step $p+1$, $\mathbf{X}^{p+1}$ is the vector containing the unknown boundary values of T or $\partial T/\partial n$ at the future time step $p+1$, and $\mathbf{B}^{p+1}$ is the vector computed from the known boundary conditions at the future time step $p+1$ and the known temperature at the future time step p or the initial condition.

Through solving Eq. (25), the unknown values of boundary nodes at the future time step $p+1$ can be determined. Based on it, the temperature at any point inside the domain Ω can be calculated according to Eq. (8) with $c(p) = 1$. The temperature distribution in domain Ω can then be determined. Subsequently, the temperature field in the whole domain for the entire time period can be obtained.

3. The inverse problem

3.1. Objective function

For the inverse geometry problem, the inner boundary shape of the furnace is regarded to be unknown, while all other parameters in the direct problem are given. Moreover, several temperature measurement points are appropriately located in the furnace wall. The inversion results can be obtained by minimizing the following objective function:

$$\min_{\boldsymbol{R}} J(\boldsymbol{R}) = \min_{\boldsymbol{R}} \sum_{i=1}^{N} \sum_{j=1}^{W} \left[T_{ij}(\boldsymbol{R}) - T_{ij}^{*} \right]^2 \tag{26}$$

where $T_{ij}(\boldsymbol{R})$ is the calculated temperature of the ith measurement point at future time step $t_j = j\Delta t_0$ under an estimated boundary shape through solving the direct problem, Δt_0 is the measurement time interval, and T_{ij}^{*} is the corresponding measurement temperature that can be simulated by the exact temperature obtained from solving the direct problem with the exact boundary shape and some random measurement errors. $\mathbf{R} = (r_1, r_2, ..., r_M)$ is the geometric parameters vector of the unknown boundary to be determined. M, N, and W are separately the numbers of the undetermined geometric parameters, measurement points, and future time step.

3.2. Conjugate gradient method

The objective function of Eq. (26) is minimized by CGM as the following iterative process: [10, 17, 44, 45]

$$\boldsymbol{R}^{k+1} = \boldsymbol{R}^{k} - \alpha^{k} \boldsymbol{d}^{k} \tag{27}$$

where α^k is the search step size from step k to $k+1$, and $\mathbf{d}^k$ is the descent direction defined as:

$$\boldsymbol{d}^{k} = \nabla J(\boldsymbol{R}^{k}) + \beta^{k} \boldsymbol{d}^{k-1} \tag{28}$$

where β^k is the conjugate coefficient given by:

$$\beta^{k} = \frac{\nabla J(\boldsymbol{R}^{k}) \nabla J^{T}(\boldsymbol{R}^{k})}{\nabla J(\boldsymbol{R}^{k-1}) \nabla J^{T}(\boldsymbol{R}^{k-1})}, \quad \text{with } \beta^{0} = 0 \tag{29}$$

where the gradient $\nabla J(\boldsymbol{R})$ is as follows:

$$\nabla J = \left[\frac{\partial J}{\partial r_1}, \frac{\partial J}{\partial r_2}, ..., \frac{\partial J}{\partial r_M} \right] \tag{30}$$

where each item is expressed as:

$$\frac{\partial J}{\partial r_n} = 2 \sum_{i=1}^{N} \sum_{j=1}^{W} \left[T_{ij}(\boldsymbol{R}) - T_{ij}{}^{*} \right] \frac{\partial T_{ij}(\boldsymbol{R})}{\partial r_n}, n = 1, 2, ..., M \tag{31}$$

The search step size α^k can be obtained by optimizing the function $J(\mathbf{R}^k - \alpha^k \mathbf{d}^k)$, namely

$$\frac{\partial J(\boldsymbol{R}^{k} - \alpha^{k} \boldsymbol{d}^{k})}{\partial \alpha^{k}} = 0 \tag{32}$$

$J(\mathbf{R}^k - \alpha^k \mathbf{d}^k)$ is the implicit function of α^k, so the exact search step size is hard to be obtained. Then, the first-order Taylor expansion is applied for $J(\mathbf{R}^k - \alpha^k \mathbf{d}^k)$, and the following expression can be concluded:

$$\alpha^{k} = \frac{\sum_{i=1}^{N} \sum_{j=1}^{W} \left[T_{ij}(\boldsymbol{R}^{k}) - T_{ij}{}^{*} \right] \nabla T_{ij} \cdot \boldsymbol{d}^{k}}{\sum_{i=1}^{N} \sum_{j=1}^{W} \left[\nabla T_{ij} \cdot \boldsymbol{d}^{k} \right]^2} \tag{33}$$

where ∇T_{ij} is the sensitivity coefficients vector written as:

$$\nabla T_{ij} = \left[\frac{\partial T_{ij}}{\partial r_1}, \frac{\partial T_{ij}}{\partial r_2}, ..., \frac{\partial T_{ij}}{\partial r_M}\right] \tag{34}$$

Conventionally, the sensitivity coefficients can be obtained by the FDM approximately, namely

$$\frac{\partial T_{ij}}{\partial r_s} \approx \frac{T_{ij}(r_1, r_2, ..., r_s + \delta r_s, ..., r_M) - T_{ij}(r_1, r_2, ..., r_s - \delta r_s, ..., r_M)}{2\delta r_s} \tag{35}$$

where δr_s is the step size of the geometric parameter r_s. The accuracy of FDM is dependent of the step size δr_s. If the step size δr_s is too large, the obtained results are not accurate enough; if it is too small, the results will diverge. Naturally, the determination of step size δr_s becomes a limiting factor for obtaining a stable solution. Furthermore, to obtain the calculated temperature $T_{ij}(r_1, r_2, ..., r_s + \delta r_s, ..., r_M)$ and $T_{ij}(r_1, r_2, ..., r_s - \delta r_s, ..., r_M)$ in Eq. (35), the direct problem is required to be solved twice additionally. If the number of inversion parameters is large, it is difficult to adopt the FDM in practical applications due to a huge amount of calculation.

3.3. Evaluation of sensitivity coefficients using CVDM

Lyness and Moler [55] proposed the CVDM in 1967. In the method, the real variable z of a function $F(z)$ is substituted with a complex number $z + \mathrm{i}h$ where h is the step size with a small number. The Taylor expansion of the function $F(z + \mathrm{i}h)$ can be stated as:

$$F(z + \mathrm{i}h) = F(z) + \mathrm{i}h\frac{\mathrm{d}F}{\mathrm{d}z} - \frac{h^2}{2}\frac{\mathrm{d}^2F}{\mathrm{d}z^2} + o(h^3) \tag{36}$$

Due to $h \ll$ z, the first-order derivative of function $F(z)$ can be expressed as:

$$\frac{\mathrm{d}F}{\mathrm{d}z} \approx \frac{\mathrm{Im}(F(z + \mathrm{i}h))}{h} \tag{37}$$

where the symbol Im indicates the imaginary part. We can see that by utilizing CVDM, the first-order derivative can be obtained by calculating the function only once. This merit is particularly competitive when the function is a complex implicit function and the calculation cost is huge.

Table 1. The first-order derivatives $F'(z)$ and relative errors with different h.

	$z = -0.5$				$z = 2.5$			
	FDM		CVDM		FDM		CVDM	
h	Numerical result	Relative error (%)	Numerical result	Relative error (%)	Numerical result	Relative error (%)	Numerical result	Relative error (%)
1.0E-01	−18.7683847	7.8984471	−16.1745682	7.0132662	−24.1835471	0.0008303	−24.1839231	0.0007245
1.0E-02	−17.4074258	0.0743667	−17.3815698	0.0742781	−24.1837461	0.0000074	−24.1837498	0.0000079
1.0E-03	−17.3946194	0.0007433	−17.3943608	0.0007433	−24.1837479	0.0000000	−24.1837480	0.0000004
1.0E-04	−17.3944914	0.0000075	−17.3944888	0.0000075	−24.1837479	0.0000000	−24.1837479	0.0000000
1.0E-05	−17.3944901	0.0000000	−17.3944901	0.0000000	−24.1837479	0.0000000	−24.1837479	0.0000000
1.0E-06	−17.3944901	0.0000000	−17.3944901	0.0000000	−24.1837479	0.0000000	−24.1837479	0.0000000
1.0E-07	−17.3944901	0.0000000	−17.3944901	0.0000000	−24.1837479	0.0000000	−24.1837479	0.0000000
1.0E-08	−17.3944901	0.0000000	−17.3944901	0.0000000	−24.1837481	0.0000008	−24.1837479	0.0000000
1.0E-09	−17.3944897	0.0000023	−17.3944901	0.0000000	−24.1837451	0.0000116	−24.1837479	0.0000000
1.0E-10	−17.3944921	0.0000115	−17.3944901	0.0000000	−24.1837447	0.0000132	−24.1837479	0.0000000
1.0E-11	−17.3944830	0.0000408	−17.3944901	0.0000000	−24.1836733	0.0003085	−24.1837479	0.0000000
1.0E-12	−17.3940831	0.0023398	−17.3944901	0.0000000	−24.1833177	0.0017789	−24.1837479	0.0000000
1.0E-13	−17.3994119	0.0282952	−17.3944901	0.0000000	−24.1762119	0.0311614	−24.1837479	0.0000000
1.0E-14	−17.3638845	0.1759500	−17.3944901	0.0000000	−24.8689906	2.8334843	−24.1837479	0.0000000
1.0E-15	−17.7635644	2.1217886	−17.3944901	0.0000000	−21.3162773	11.8570149	−24.1837479	0.0000000
1.0E-16	−17.7635642	2.1217874	−17.3944901	0.0000000	0	100.0000000	−24.1837479	0.0000000
1.0E-17 ∼ 1.0E-100	0	100.0000000	−17.3944901	0.0000000	0	100.0000000	−24.1837479	0.0000000

To verify the validity of CVDM, a complicated function is taken as:

$$F(z) = \frac{\sin(3z)}{1-e^{2z}} + e^z - 2z^3 + z - \frac{1}{z^2} \tag{38}$$

The analytical solution of the first-order derivative of $F(z)$ is equal to:

$$F'(z) = \frac{2e^{2z}\sin(3z)}{(1-e^{2z})^2} + \frac{3\cos(3z)}{1-e^{2z}} + e^z - 6z^2 + \frac{2}{z^3} + 1 \tag{39}$$

The exact values of first-order derivatives $F'(-0.5)$ and $F'(2.5)$ are, respectively, -17.3944901 and -24.1837479 by Eq. (39). The numerical results of FDM and CVDM as well as the relative errors compared to the exact results are reported in Table 1. According to Table 1, the first-order derivatives can be calculated precisely for the step size h between 10^{-5} and 10^{-100} by CVDM. It is obvious that the calculation results of CVDM are independent of the step size h, because the results are still accurate when h is as small as 10^{-100}. However, the calculation values of FDM depend on the step size h, which are accurate only for h between 10^{-5} and 10^{-7}, and will be wrong and meaningless when h is less than 10^{-17}. Therefore, the utilization of CVDM can improve the accuracy and efficiency of the calculation of sensitivity coefficients in the iteration process.

In this work, the formula for determining the sensitivity coefficients vector in Eq. (34) is as follows, and the step size is taken as $h = 10^{-10}$:

$$\frac{\partial T_{ij}}{\partial r_s} \approx \frac{\mathrm{Im}(T_{ij}(r_1, r_2, \ldots, r_s + \mathrm{i}h, \ldots, r_M))}{h} \tag{40}$$

3.4. Stopping criterion

For the inverse iterative process without measurement errors, the stopping criterion is taken as follows:

$$J(\boldsymbol{R}) = \sum_{i=1}^{N}\sum_{j=1}^{W}\left[T_{ij}(\boldsymbol{R}) - T_{ij}^*\right]^2 < \varepsilon \tag{41}$$

where ε is a specified small positive number.

However, measurement errors always exist in practice applications. Taking into account measurement errors, the measurement temperature can be given as:

$$T_{ij}{}^* = T_{ij}^{exact} + \sigma\omega \tag{42}$$

where T_{ij}^{exact} is the real temperature of the ith measurement point at time t_j, which is obtained through solving the direct problem with the real boundary shape. ω is a random variable that adheres to a normal distribution with zero mean and unit standard deviation within $(-2.576, 2.576)$. Additionally, σ is the standard deviation of measurement error. The stopping criterion ε can be expressed as:

$$\varepsilon = \sum_{i=1}^{N}\sum_{j=1}^{W}\sigma^2 = NW\sigma^2 \tag{43}$$

Thus, the stopping criterion can be determined by Eqs. (41) and (43).

3.5. Procedure of inverse calculation

The procedure of inverse calculation for estimating the boundary shape is stated as follows:

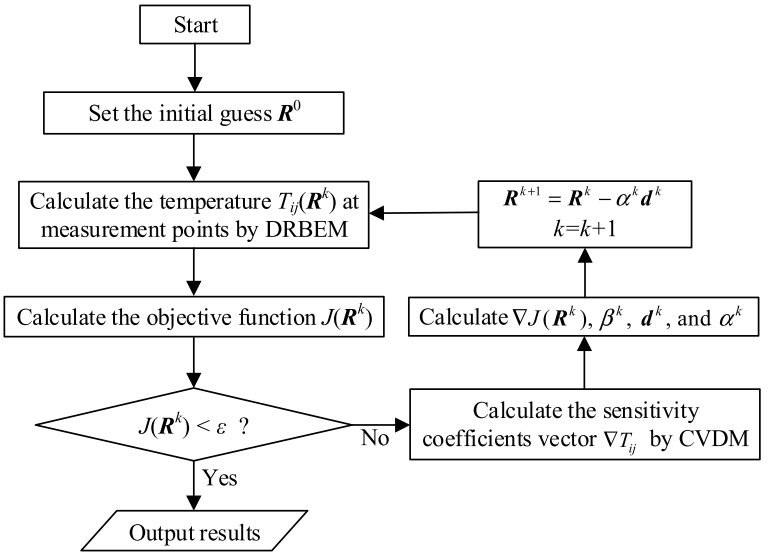

Figure 2. The flowchart of CGM for boundary identification.

Step 1. Set the initial guess values for the unknown geometric parameters $\boldsymbol{R}^0$. Use constant elements to discretize the geometry boundary. Take the iterative step index $k = 0$.

Step 2. Solve the direct problem of transient heat conduction using the DRBEM to determine the computed temperature $T_{ij}(\boldsymbol{R}^k)$ at measurement points.

Step 3. Compute the objective function $J(\mathbf{R}^k)$. Check whether the stopping criteria is met. If it is achieved, stop the calculation. Otherwise, go on.

Step 4. Calculate the sensitivity coefficients vector ∇T_{ij} by CVDM. Calculate the gradient $\nabla J(\mathbf{R}^k)$ and conjugate coefficient β^k, respectively. Then calculate the descent direction $\mathbf{d}^k$.

Step 5. Calculate the search step size α^k, and next calculate the unknown geometric parameters $\boldsymbol{R}^{k+1}$ of the iteration step $k+1$.

Step 6. Update step k by $k+1$, and go back to Step 2.

Figure 2 shows the calculation flowchart of CGM for boundary identification.

4. Results and discussion

To study the accuracy of inversion results, the maximum relative error (MRE) and average relative error (ARE) between the real and identified geometry shapes are, respectively, written as:

$$\mathrm{MRE} = \max\left|\frac{r_i - r_i^*}{r_i^*}\right| \times 100\%, \quad i = 1, 2, \ldots, M \tag{44}$$

$$\mathrm{ARE} = \frac{1}{M}\sum_{i=1}^{M}\left|\frac{r_i - r_i^*}{r_i^*}\right| \times 100\% \tag{45}$$

where r_i and r_i^* are the estimated and exact geometric parameters, respectively.

In the following numerical examples, the thermal diffusivity is taken to be unity. The boundaries Γ_{in} and Γ_{out} of the furnace wall are all discretized by 30 constant elements, while the radius of boundary Γ_{out} is $r_{out} = 1.0$ m. The number of undetermined geometric parameters is $M = 30$,

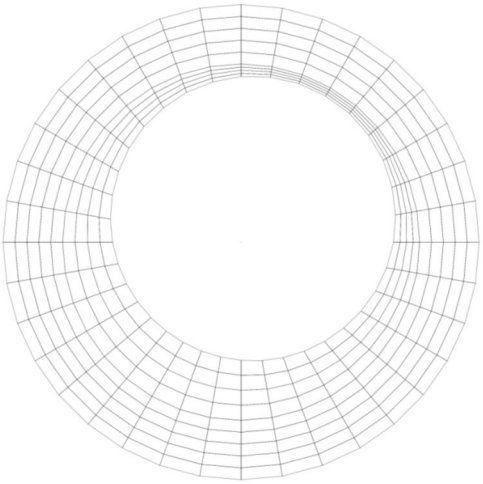

Figure 3. The computational mesh of FEM in the furnace wall.

the initial temperature condition is T_0=30 °C, and the temperature of boundary Γ_{out} is T_{out} = 30 °C.

4.1. The influence factors for solving the direct problem

Consider that the inner boundary shape of the furnace is an eccentric circle given as:

$$(x-0.05)^2+(y-0.1)^2=0.6^2 \tag{46}$$

The inner boundary temperature is chosen to be $T_{in}=30+16\sin(\pi t/4)\times e^{-0.02t}$, and the time step size is taken as Δt= 0.5s. It is hard to find the analytical solution to this problem for the temperature distribution. To test the accuracy of the DRBEM, the results from using the FEM in NX12.0 software are taken as the reference values. In the FEM model, the problem domain is discretized by 324 quadrilateral elements as shown in Figure 3. In addition, the effect of different radial-basis functions (case 1: $f=1+r$, case 2: $f=1+r+r^2$, and case 3: $f=r^2lnr$) for the DRBEM is also investigated. The temperatures of some points are reported in Table 2. According to Table 2, it can be seen that the results obtained by the DRBEM and FEM agree well with each other, and different radial-basis functions have little influence on the accuracy of the DRBEM in this example. This indicates that the DRBEM is a highly accurate method for solving the transient heat conduction problem. Moreover, the radial-basis function $f=1+r$ has a simple form and is widely used because of its high numerical accuracy and efficiency [56]. Therefore, this form is chosen as the radial-basis function for the following numerical calculations in this study.

In order to investigate the effect of the number of internal collocation points, the numbers of $L=12$, 24, and 36 are considered. When the number is $L=12$, the internal collocation points are evenly arranged at $r(\theta)=0.95$ m in the domain Ω; when $L=24$, evenly arranged at $r(\theta)$= 0.95 m and 0.90 m; when $L=36$, evenly arranged at $r(\theta)=0.95$ m, 0.90 m, and 0.85 m. The temperature evolution over time at point (0.95 m, 0) with different numbers of internal collocation points are shown in Figure 4. From the results, it can be seen that the number of internal collocation points varying from $L=12$ to 36 has little effect on the calculated transient temperatures in the furnace wall. In the subsequent numerical examples, $L=36$ internal collocation points uniformly distributed at $r(\theta)=0.95$ m, 0.90 m, and 0.85 m are used.

The time step sizes are, respectively, set to be $\Delta t=0.25$ s, 0.5 s, and 2.5 s to simulate the temperature evolution over time. The results at point (0, 0.95 m) with different time step sizes are shown in Figure 5. It is clear that the calculated results for $\Delta t=0.25$ s and 0.5 s are almost the

Table 2. Comparison of the temperatures of the FEM and the DRBEM with different radial-basis functions.

	$t = 5$ s				$t = 10$ s				$t = 15$ s			
Point position (m)	Case 1 (°C)	Case 2 (°C)	Case 3 (°C)	FEM (°C)	Case 1 (°C)	Case 2 (°C)	Case 3 (°C)	FEM (°C)	Case 1 (°C)	Case 2 (°C)	Case 3 (°C)	FEM (°C)
(0.85, 0)	26.403	26.405	26.401	26.395	34.669	34.668	34.669	34.676	26.972	26.971	26.973	26.968
(0.90, 0)	27.698	27.701	27.697	27.695	32.976	32.975	32.976	32.995	28.059	28.057	28.060	28.055
(0.95, 0)	28.930	28.932	28.925	28.920	31.393	31.393	31.394	31.405	29.096	29.095	29.099	29.087
(0, 0.85)	25.569	25.571	25.566	25.570	35.720	35.719	35.720	35.720	26.305	26.304	26.307	26.308
(-0.85, 0)	27.395	27.397	27.397	27.384	33.415	33.415	33.415	33.429	27.764	27.763	27.763	27.754
(0, −0.85)	27.713	27.715	27.719	27.702	33.010	33.009	33.008	33.028	28.018	28.017	28.015	28.007

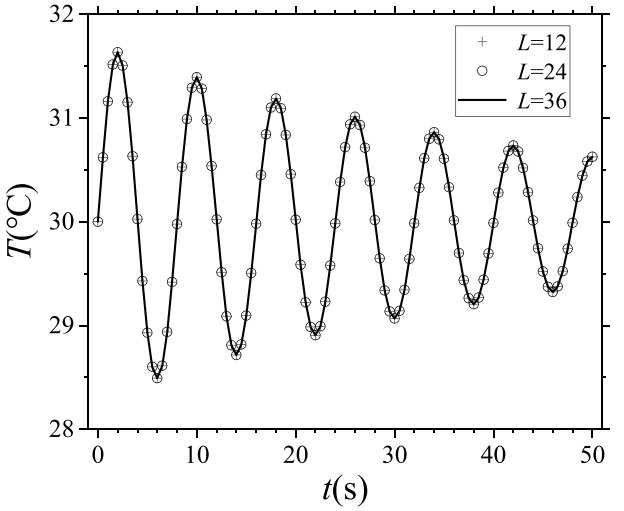

Figure 4. The temperature evolution over time at point (0.95 m, 0) with different numbers of internal collocation points.

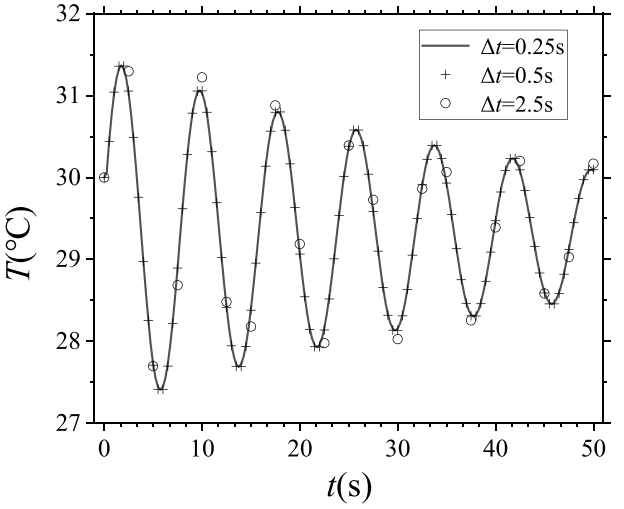

Figure 5. The temperature evolution over time at point (0, 0.95 m) with different time step sizes.

same, while those for $\Delta t = 2.5\,\mathrm{s}$ deviate slightly from the formers. The time step size is chosen as $\Delta t = 0.5\,\mathrm{s}$ in the following inverse estimation of this article.

4.2. Comparison with the conventional CGM

Consider that the inner boundary shape of the furnace is expressed as:

$$r_{in}^{*}(\theta) = \sqrt{(0.1\sin\theta + 0.4)^2 + (0.1\cos\theta + 0.45)^2} \tag{47}$$

The inner boundary temperature is chosen to be $T_{in} = 30 + 15te^{-0.1t}$. The initial guess is $\boldsymbol{r}^0 = 0.8$ m, the measurement error is $\sigma = 0.3\,^{\circ}\mathrm{C}$, and the measurement time interval is taken as $\Delta t_0 = 3\,\mathrm{s}$. The future time step is $W = 4$, and $N = 12$ measurement points are evenly located in the domain Ω along $r(\theta) = 0.90\mathrm{m}$. Thus, there are 48 measurement temperatures, numbered from 1 to 48.

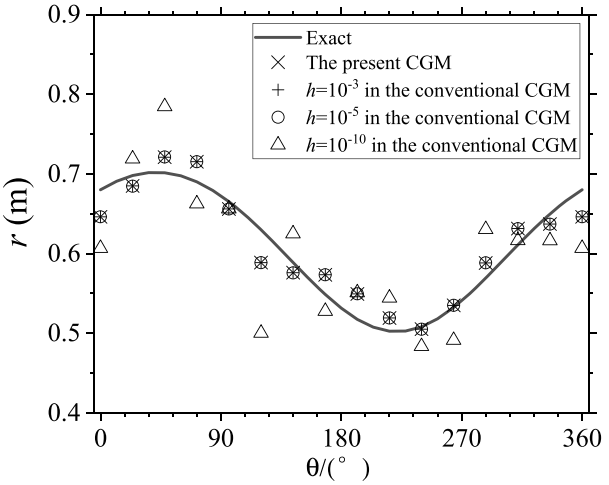

Figure 6. Inversion solutions with different step sizes h for the calculation of sensitivity coefficients ($\sigma = 0.3\,^{\circ}\mathrm{C}$).

Table 3. Relative errors with different step sizes h for the calculation of sensitivity coefficients.

Optimization method	Step size h	Number of iterations	Maximum relative error (%)	Average relative error (%)
The present CGM	10^{-3}, 10^{-5}, 10^{-10}, and 10^{-15}	4	7.19	3.25
The conventional CGM	10^{-3}	4	7.19	3.25
	10^{-5}	4	7.21	3.25
	10^{-10}	17	20.57	6.63
	10^{-15}	Divergence	Divergence	Divergence

Different values of step size ($h = 10^{-3}$, 10^{-5}, 10^{-10}, and 10^{-15}) are used to calculate the sensitivity coefficients for the present CGM and the conventional CGM. In the present CGM, the sensitivity coefficients are calculated by the CVDM corresponding to Eq. (40). While in the conventional CGM, they are calculated by the FDM corresponding to Eq. (35). The estimated results are presented in Figure 6, with the corresponding relative errors reported in Table 3. According to the results, the present CGM can obtain accurate results no matter how the step size h is chosen, and the precision of the results with different step sizes h is exactly the same. In the conventional CGM, when $h = 10^{-3}$ and 10^{-5}, the estimated results are in good agreement with those of the present CGM. Meanwhile, as h decreases to 10^{-10}, the inversion accuracy decreases significantly, and when h is 10^{-15}, the results are divergent. Obviously, we can see that the present CGM is independent of the step size h. Nevertheless, the conventional CGM is strongly influenced by the step size h, and the results will diverge when the value of h is small. To find the reason for the low accuracy or even divergence of the estimated results in the conventional CGM, we calculate the sensitivity coefficients of the 48 measurement temperatures to the first geometric parameter r_1 at the first iteration, as shown in Table 4. From Table 4, it can be seen that the sensitivity coefficients for the present CGM with different step sizes h are the same, which indicates that the sensitivity coefficients are calculated exactly. However, as the step size h decreases, the calculation of the sensitivity coefficients for the conventional CGM is not accurate enough or even incorrect, resulting in poor accuracy or even divergence of the results.

Additionally, in the present CGM, the number of iterations is low and the calculation time is less than 5 min by using the PC with an Intel Core i5-5200U processor and 8 GB memory. During each iteration in the inverse process, the computation time of the conventional CGM is approximately twice as long as that of the present CGM, due to the fact that the FDM requires solving the direct problem in Eq. (35) twice. Therefore, the findings above indicate that the present CGM is more stable and efficient than the conventional CGM.

Table 4. The sensitivity coefficients of the 48 measurement temperatures to the first geometric parameter r_1.

No. of Measurement temperature	The present CGM	The conventional CGM			
	$h=10^{-3}$, 10^{-5}, 10^{-10}, and 10^{-15}	$h=10^{-3}$	$h=10^{-5}$	$h=10^{-10}$	$h=10^{-15}$
1	4.824E + 01	4.824E + 01	4.824E + 01	5.165E + 01	4.263E + 01
2	6.274E−02	6.289E−02	6.727E−02	3.727E + 00	7.105E + 00
3	−1.401E−03	−1.236E−03	4.231E−03	4.155E + 00	1.421E + 01
4	4.103E−03	4.276E−03	1.021E−02	4.143E + 00	−1.421E + 01
5	8.096E−03	8.279E−03	1.449E−02	4.208E + 00	−1.421E + 01
6	1.301E−02	1.320E−02	1.932E−02	4.274E + 00	−2.132E + 01
7	1.533E−02	1.553E−02	2.161E−02	4.408E + 00	3.908E + 01
8	1.301E−02	1.320E−02	1.932E−02	4.281E + 00	2.487E + 01
9	8.096E−03	8.279E−03	1.449E−02	4.221E + 00	−1.066E + 01
10	4.103E−03	4.276E−03	1.021E−02	4.171E + 00	−1.776E + 01
11	−1.401E−03	−1.236E−03	4.231E−03	4.172E + 00	2.132E + 01
12	6.274E−02	6.289E−02	6.727E−02	3.740E + 00	1.776E + 01
13	7.114E + 01	7.114E + 01	7.114E + 01	7.262E + 01	8.171E + 01
14	9.785E−02	9.792E−02	9.982E−02	1.690E + 00	−1.066E + 01
15	2.690E−03	2.762E−03	5.132E−03	1.808E + 00	1.421E + 01
16	4.477E−03	4.552E−03	7.126E−03	1.803E + 00	1.776E + 01
17	6.785E−03	6.865E−03	9.558E−03	1.832E + 00	1.421E + 01
18	8.360E−03	8.443E−03	1.110E−02	1.859E + 00	−7.105E + 00
19	9.933E−03	1.002E−02	1.266E−02	1.919E + 00	−2.132E + 01
20	8.360E−03	8.443E−03	1.110E−02	1.862E + 00	2.132E + 01
21	6.785E−03	6.865E−03	9.558E−03	1.837E + 00	2.132E + 01
22	4.477E−03	4.552E−03	7.126E−03	1.815E + 00	−1.421E + 01
23	2.690E−03	2.762E−03	5.132E−03	1.816E + 00	4.619E + 01
24	9.785E−02	9.792E−02	9.982E−02	1.696E + 00	−1.066E + 01
25	7.893E + 01	7.893E + 01	7.893E + 01	7.925E + 01	5.329E + 01
26	1.106E−01	1.106E−01	1.110E−01	4.581E−01	1.421E + 01
27	4.754E−03	4.770E−03	5.281E−03	3.996E−01	2.132E + 01
28	4.382E−03	4.398E−03	4.953E−03	3.969E−01	−3.553E + 00
29	5.610E−03	5.628E−03	6.209E−03	4.046E−01	−1.776E + 01
30	5.248E−03	5.266E−03	5.838E−03	4.090E−01	−3.197E + 01
31	6.305E−03	6.323E−03	6.892E−03	4.233E−01	2.487E + 01
32	5.248E−03	5.266E−03	5.838E−03	4.102E−01	2.132E + 01
33	5.610E−03	5.628E−03	6.209E−03	4.057E−01	2.132E + 01
34	4.382E−03	4.398E−03	4.953E−03	3.996E−01	1.066E + 01
35	4.754E−03	4.770E−03	5.281E−03	4.015E−01	2.132E + 01
36	1.106E−01	1.106E−01	1.110E−01	4.595E−01	−1.776E + 01
37	7.789E + 01	7.789E + 01	7.789E + 01	7.756E + 01	5.329E + 01
38	1.101E−01	1.101E−01	1.097E−01	−2.482E−01	−1.421E + 01
39	5.567E−03	5.551E−03	5.008E−03	−4.004E−01	3.553E + 00
40	4.035E−03	4.018E−03	3.428E−03	−4.014E−01	−7.105E + 00
41	4.588E−03	4.570E−03	3.953E−03	−4.060E−01	1.066E + 01
42	3.188E−03	3.169E−03	2.559E−03	−4.140E−01	−2.842E + 01
43	3.890E−03	3.870E−03	3.266E−03	−4.253E−01	3.553E + 00
44	3.188E−03	3.169E−03	2.559E−03	−4.147E−01	−3.553E + 00
45	4.588E−03	4.570E−03	3.953E−03	−4.072E−01	−1.066E + 01
46	4.035E−03	4.018E−03	3.428E−03	−4.039E−01	−1.421E + 01
47	5.567E−03	5.551E−03	5.008E−03	−4.026E−01	5.684E + 01
48	1.101E−01	1.101E−01	1.097E−01	−2.494E−01	−7.105E + 00

4.3. The effect of the measurement time interval

Suppose that the inner geometry boundary of the furnace is given by:

$$r_{in}^{*}(\theta) = 0.6 + 0.1\sin(\theta - 45^{\circ}) \tag{48}$$

The inner boundary temperature is imposed as $T_{in} = 20 + 10\cos(\pi t/2) \times e^{-0.01t}$. The future time step is $W = 4$, the measurement error is $\sigma = 0.1\,^{\circ}\mathrm{C}$, and the initial guess is $\boldsymbol{r}^0 = 0.4$ m. The $N = 12$ measurement points are located in the domain Ω along $r(\theta) = 0.95$m homogeneously. The measurement time intervals are, respectively, chosen as $\Delta t_0 = 3$ s, 5s, and 7s to survey the

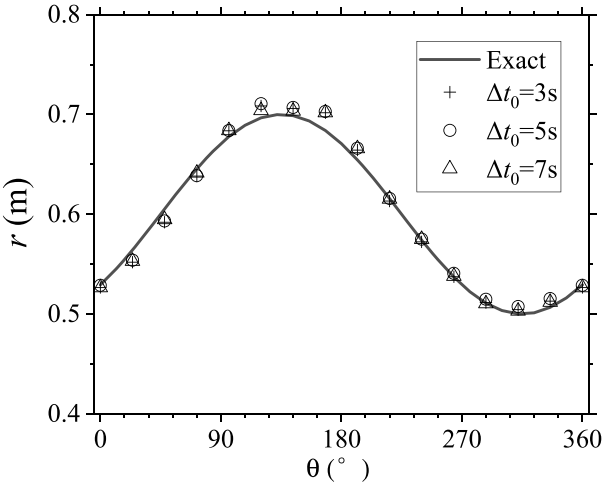

Figure 7. Inversion solutions with different measurement time intervals (σ= 0.1 °C).

Table 5. Relative errors with different measurement time intervals.

Measurement time interval Δt_0 (s)	Number of iterations	Maximum relative error (%)	Average relative error (%)
3	5	4.07	1.09
5	5	4.31	1.24
7	5	4.02	0.92

influence on the results. The inversion results of the unknown boundary shape are presented in Figure 7, with the corresponding relative errors reported in Table 5. According to the above results, the proposed method can obtain accurate results no matter how the measurement time intervals are chosen. In the following examples, the measurement time interval is taken as Δt_0= 3 s.

4.4. The effect of the future time step

The unknown geometry boundary of the furnace is assumed as follows:

$$(x-0.1)^2+y^2=0.65^2 \tag{49}$$

The inner boundary temperature is given by $T_{in}=30+12(x+y)\sin(\pi t/2)\times e^{-0.05t}$. The N= 12 measurement points are located in the domain Ω along $r(\theta)=0.90$m uniformly, the measurement error is σ = 0.2 °C, and the initial guess is $\boldsymbol{r}^0$ = 0.8 m. The future time steps are taken to be W= 4, 8, and 12 to investigate the effect on the inversion results. The inversion results of the unknown geometry boundary are presented in Figure 8, with the corresponding relative errors reported in Table 6. Based on the results, we can see that the accuracy of the inversion results can be slightly improved with the increase of the future time step. Moreover, the inversion results are all satisfactory for different future time steps, which indicate that the proposed approach reduces the dependence of inversion results on the future time step and is suitable for appropriately shortening the measurement time span. In the following cases, the future time step is taken as W= 4.

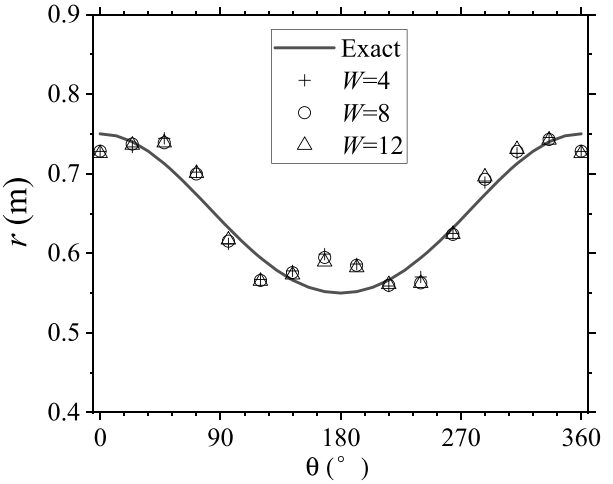

Figure 8. Inversion solutions with different future time steps (σ= 0.2 °C).

Table 6. Relative errors with different future time steps.

Future time step W	Number of iterations	Maximum relative error (%)	Average relative error (%)
4	4	8.56	3.20
8	4	7.77	3.07
12	4	6.79	2.98

4.5. The effect of the initial guess

The unknown geometry boundary of the furnace is assumed as an ellipse:

$$\frac{x^2}{0.4^2}+\frac{y^2}{0.6^2}=1 \tag{50}$$

In this example, the inner boundary temperature is assumed as $T_{in}=30+(t+t^2)e^{-0.1t}$, the measurement error is $\sigma=0$, and the $N=12$ measurement points are arranged along $r(\theta)=0.85$m homogeneously. The initial guesses are set to be $\boldsymbol{r}^0=0.2$ m, 0.4 m, and 0.6 m, respectively. The inversion results are shown in Figure 9, while the corresponding relative errors are presented in Table 7. It is clear that the inversion results are satisfactory, even for the initial guess deviating greatly from the actual shape.

Next, the measurement error is taken as $\sigma=0.3\,^{\circ}$C, and the other parameters in the inversion process are the same as $\sigma=0$. The results are reported in Figure 10 and Table 7. We can see that the inversion results are slightly worse than those for $\sigma=0$, but they are still accurate enough in practical applications.

From the above results, it can be concluded that the proposed approach in this article is insensitive to the initial guess, regardless of the presence or absence of measurement errors.

4.6. The effect of the measurement error

The inner geometry boundary of the furnace is assumed to be as follows:

$$r_{in}^{*}(\theta)=0.6+0.1\cos(2\theta-45^{\circ}) \tag{51}$$

The inner boundary temperature is specified as $T_{in}=30+10te^{-0.1t}$. The $N=12$ measurement points are distributed along $r(\theta)=0.90$m regularly, and the initial guess is $\boldsymbol{r}^0=0.8$ m. The measurement errors are respectively chosen to be σ= 0, 0.1 °C, 0.3 °C, and 0.5 °C. Figure 11 and

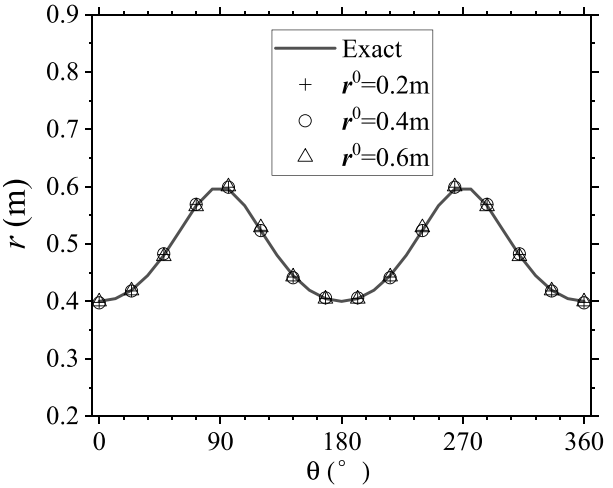

Figure 9. Inversion solutions with different initial guesses ($\sigma = 0$).

Table 7. Relative errors with different initial guesses.

Measurement error σ (°C)	Initial guess R^0 (m)	Number of iterations	Maximum relative error (%)	Average relative error (%)
0	0.2	15	0.52	0.31
	0.4	6	0.73	0.35
	0.6	12	0.85	0.44
0.3	0.2	3	7.20	3.15
	0.4	2	4.39	2.33
	0.6	2	4.81	1.92

Table 8 show the effect of the measurement error on the inversion results. From the results, it can be seen that the estimated geometry boundary fits well with the real shape for $\sigma = 0$. When measurement errors exist, the estimated geometry boundary will deviate slightly from the real shape, the degree of deviation depending on the size of the measurement error. The relative errors of the inversion results increase with the measurement error increasing from 0 to 0.5 °C. Moreover, the inversion results remain acceptable even for a large measurement error $\sigma = 0.5$ °C.

4.7. The effect of the number of measurement points

Consider that the inner geometry boundary of the furnace is expressed as follows:

$$r_{in}^{*}(\theta) = \begin{cases} 0.5 + 0.2\theta/180, & 0^\circ \le \theta \le 180^\circ \\ 0.9 - 0.2\theta/180, & 180^\circ \le \theta \le 360^\circ \end{cases} \tag{52}$$

The inner boundary temperature is set as $T_{in} = 30(1+t)e^{-0.2t}$, the initial guess is $\boldsymbol{r}^0 = 0.7$ m, and the measurement error is $\sigma = 0.3$ °C. The numbers of measurement points are chosen to be $N = 12$, 24, and 36, respectively. When the number is $N = 12$, the measurement points are uniformly distributed along $r(\theta) = 0.85$m; when $N = 24$, uniformly distributed along $r(\theta) = 0.85$ m and 0.90 m; when $N = 36$, uniformly distributed along $r(\theta) = 0.85$ m, 0.90 m, and 0.95 m. The inversion results and corresponding relative errors are presented in Figure 12 and Table 9, respectively. From the results, we can see that the accuracy of the inversion results can be improved as the number of measurement points increases. Thus, in practical applications where the measurement error cannot be reduced significantly, better inversion results can also be obtained by increasing the number of measurement points. However, the more measurement

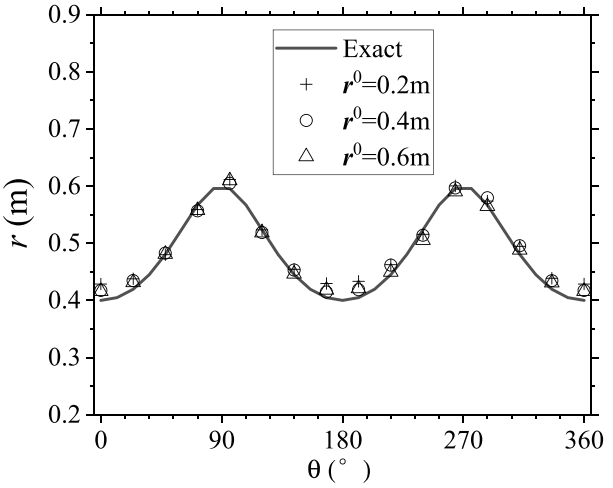

Figure 10. Inverse solutions with different initial guesses (σ= 0.3 °C).

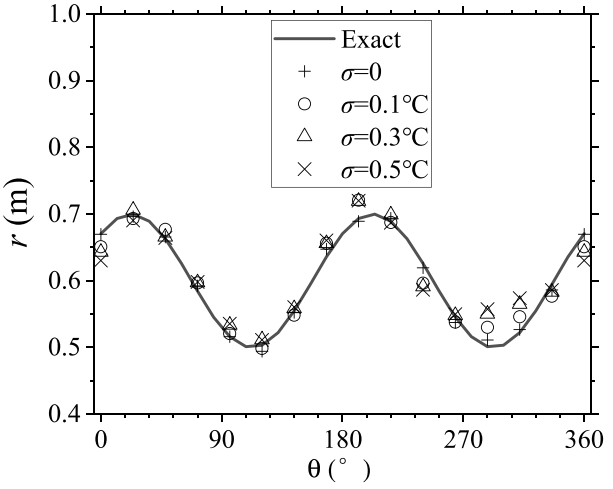

Figure 11. Inverse solutions with different measurement errors.

Table 8. Relative errors with different measurement errors.

Measurement error σ (°C)	Number of iterations	Maximum relative error (%)	Average relative error (%)
0	13	1.96	0.97
0.1	5	5.77	2.52
0.3	3	9.79	3.24
0.5	3	11.22	3.71

points there are, the less improvement in the inversion results. In this case, the $N = 12$ measurement points are enough to get satisfactory results.

4.8. The effect of the position of measurement points

Suppose that the unknown inner boundary shape of the furnace has the expression as follows:

$$r_{in}^{*}(\theta) = 0.5 + 0.2(\theta/180 - 1)^2 \tag{53}$$

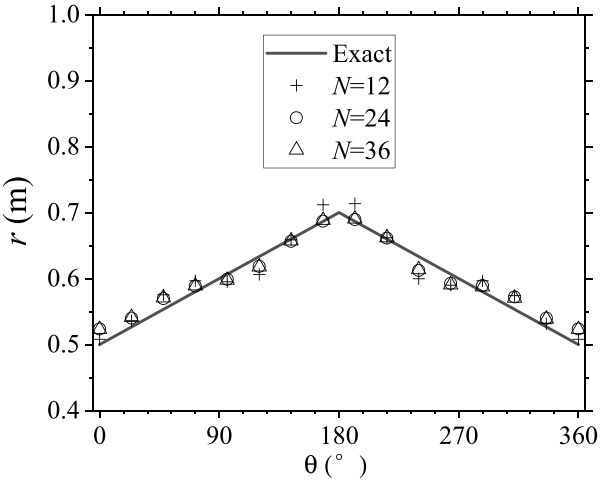

Figure 12. Inversion solutions with various numbers of measurement points (σ= 0.3 °C).

Table 9. Relative errors with various numbers of measurement points.

Measurement points number *N*	Number of iterations	Maximum relative error (%)	Average relative error (%)
12	3	7.54	2.68
24	2	7.21	1.84
36	2	7.20	1.84

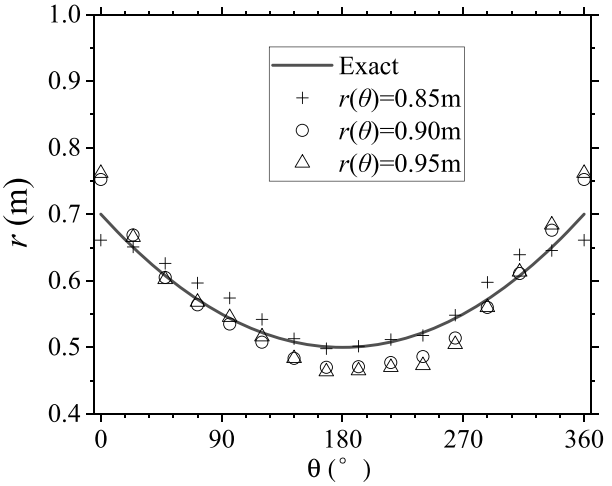

Figure 13. Inversion solutions with different positions of measurement points (σ= 0.2 °C).

Table 10. Relative errors with different positions of measurement points.

Measurement points position $r(\theta)$ (m)	Number of iterations	Maximum relative error (%)	Average relative error (%)
0.85	4	5.59	2.24
0.90	3	7.45	3.79
0.95	3	9.45	4.22

The inner boundary temperature is assumed to be $T_{in} = 30 + t$. The initial guess is given as $\boldsymbol{r}^0 = 0.4$ m, and the measurement error is $\sigma = 0.2\,^{\circ}$C. The $N = 12$ measurement points are evenly spaced along $r(\theta) = 0.85$ m, 0.90 m, and 0.95 m, respectively. Figure 13 and Table 10 illustrate

the inversion results and corresponding relative errors, respectively. From Figure 13 and Table 10, it can be found that the precision of the inversion results is related to the position of measurement points. The relative errors of the results increase as the distance between the measurement points and the unknown boundary increases. Therefore, the measurement points should be distributed as close as possible to the unknown boundary for better estimation results. Furthermore, the unknown geometry boundary can be satisfactorily identified regardless of where the measurement points are located.

5. Conclusions

The DRBEM and CGM are combined to estimate the unknown geometry boundary of a furnace under transient heat conduction. During the iteration process in CGM, the sensitivity coefficients are accurately calculated using CVDM, which is independent of the step size. The accuracy of DRBEM in solving the direct problem is examined by the influencing factors of radial-basis function, the number of internal collocation points, and time step size. To test the effectiveness of the proposed approach, several typical numerical examples have been considered, in which the inner boundary shapes and boundary conditions have different and complex functional forms. The numerical results show that the proposed approach is accurate and stable for estimating the unknown geometry boundary of the furnace with few iteration steps and a short calculation time. This approach is insensitive to the measurement time interval, future time step, initial guess, and measurement error. The inversion results become more accurate with the increase in the number of measurement points and the decrease in the distance between the measurement points and the unknown boundary.

Disclosure statement

The authors declare that they have no known competing financial interests or personal relationships that could have appeared to influence the work reported in this article.

References

[1] W. W. Han, H. B. Chen and T. Lu, "Estimation of the time-dependent convective boundary condition in a horizontal pipe with thermal stratification based on inverse heat conduction problem," *Int. J. Heat Mass Transfer*, vol. 132, pp. 723–730, 2019. DOI: 10.1016/j.ijheatmasstransfer.2018.02.119.

[2] C. Lv, G. Wang and H. Chen, "Estimation of time-dependent thermal boundary conditions and online reconstruction of transient temperature field for boiler membrane water wall," *Int. J. Heat Mass Transfer*, vol. 147, pp. 118955, 2020. DOI: 10.1016/j.ijheatmasstransfer.2019.118955.

[3] T. Hikata and H. Fujimoto, "Evaluating surface heat flux in planar water-jet cooling of moving hot solid by inversely solving steady-state heat conduction," *Int. J. Heat Mass Transfer*, vol. 197, pp. 123364, 2022. DOI: 10.1016/j.ijheatmasstransfer.2022.123364.

[4] L. Qiu, J. Lin, F. Wang, Q.-H. Qin and C.-S. Liu, "A homogenization function method for inverse heat source problems in 3D functionally graded materials," *Appl. Math. Modelling*, vol. 91, pp. 923–933, 2021. DOI: 10.1016/j.apm.2020.10.012.

[5] M. J. Huntul, "Identifying an unknown heat source term in the third-order pseudo-parabolic equation from nonlocal integral observation," *Int. Commun. Heat Mass Transfer*, vol. 128, pp. 105550, 2021. DOI: 10.1016/j.icheatmasstransfer.2021.105550.

[6] S. Somasundharam and K. S. Reddy, "Inverse analysis for simultaneous estimation of temperature dependent thermal properties of isotropic materials," *Therm. Sci. Eng. Prog.*, vol. 20, no. 8, pp. 100728, 2020. DOI: 10.1016/j.tsep.2020.100728.

[7] Y. Zhou and X. X. Hu, "Two methods for estimation of temperature-dependent thermal conductivity based on constant element approximation," *Int. J. Therm. Sci.*, vol. 135, pp. 104–116, 2019. DOI: 10.1016/j.ijthermalsci.2018.09.008.

[8] F. Mohebbi, B. Evans and T. Rabczuk, "Solving direct and inverse heat conduction problems in functionally graded materials using an accurate and robust numerical method," *Int. J. Therm. Sci.*, vol. 159, pp. 106629, 2021. DOI: 10.1016/j.ijthermalsci.2020.106629.

[9] V. Tahmasbi and S. Noori, "Inverse identification of temperature-dependent thermal conductivity components in an orthotropic charring composite," *Appl. Therm. Eng.*, vol. 183, pp. 116219, 2021. DOI: 10.1016/j.applthermaleng.2020.116219.

[10] J. Y. Tan, J. M. Zhao and L. H. Liu, "Meshless method for geometry boundary identification problem of heat conduction," *Numer. Heat Transfer B Fundam.*, vol. 55, no. 2, pp. 135–154, 2009. DOI: 10.1080/10407790802605166.

[11] M. Higuera, J. M. Perales, M. L. Rapún and J. M. Vega, "Solving inverse geometry heat conduction problems by postprocessing steady thermograms," *Int. J. Heat Mass Transfer*, vol. 143, pp. 118490, 2019. DOI: 10.1016/j.ijheatmasstransfer.2019.118490.

[12] Y. Li, G. Wang, H. Chen, Z. Zhu and D. Zhang, "A decentralized fuzzy inference method for the inverse geometry heat conduction problem," *Appl. Therm. Eng.*, vol. 106, pp. 109–116, 2016. DOI: 10.1016/j.applthermaleng.2016.05.161.

[13] G. Jiang, C. Tan, W. Jiang, K. Yang, W. Wang and X. Gao, "Shape reconstruction in transient heat conduction problems based on radial integration boundary element method," *Int. J. Heat Mass Transfer*, vol. 191, pp. 122830, 2022. DOI: 10.1016/j.ijheatmasstransfer.2022.122830.

[14] B. Yu, P. Hua, P. Wei, G. Cao and B. Wang, "The identification of voids and inclusions based on the parameter level set method using boundary data," *Appl. Math. Modelling*, vol. 112, pp. 505–539, 2022. DOI: 10.1016/j.apm.2022.08.015.

[15] J. V. Beck, B. Blackwell and R. S. Clair, *Inverse Heat Conduction: Ill-Posed Problems*, New York, NY: Wiley, 1985,

[16] S. Wang, S. C. Lin and Y. C. Yang, "Geometry estimation for the inner surface in a furnace wall made of functionally graded materials," *Int. Comm. Heat Mass Transfer*, vol. 67, pp. 1–7, 2015. DOI: 10.1016/j.icheatmasstransfer.2015.06.012.

[17] W. L. Chen, Y. C. Yang, H. L. Lee and W. J. Chang, "Estimation for inner surface geometry of a two-layer-wall furnace with inner wall made of functionally graded materials," *Int. Commun. Heat Mass Transfer*, vol. 97, pp. 143–150, 2018. DOI: 10.1016/j.icheatmasstransfer.2018.07.009.

[18] C. R. Su and C. K. Chen, "Geometry estimation of the furnace inner wall by an inverse approach," *Int. J. Heat Mass Transfer*, vol. 50, no. 19–20, pp. 3767–3773, 2007. DOI: 10.1016/j.ijheatmasstransfer.2007.02.024.

[19] C. K. Chen and C. R. Su, "Inverse estimation for temperatures of outer surface and geometry of inner surface of furnace with two layer walls," *Energy. Convers. Manage*, vol. 49, no. 2, pp. 301–310, 2008. DOI: 10.1016/j.enconman.2007.06.010.

[20] C. R. Su, C. K. Chen, W. L. Liu and H. Y. Lai, "Estimation for inner surface geometry of furnace wall using inverse process combined with grey prediction model," *Int. J. Heat Mass Transfer*, vol. 52, no. 15–16, pp. 3595–3605, 2009. DOI: 10.1016/j.ijheatmasstransfer.2009.02.037.

[21] G. Wang, Z. Luo, L. Zhu, H. Chen and L. Zhang, "Fuzzy estimation for temperature distribution of furnace inner surface," *Int. J. Therm. Sci.*, vol. 51, pp. 84–90, 2012. DOI: 10.1016/j.ijthermalsci.2011.07.015.

[22] B. Yu, H. L. Zhou, Q. Gao and J. Yan, "Geometry boundary identification of the furnace inner wall by BEM without iteration," *Numer. Heat Transfer A Appl.*, vol. 69, no. 11, pp. 1253–1262, 2016. DOI: 10.1080/10407782.2016.1139965.

[23] B. Yu, W. Yao, Q. Gao, H. Zhou and C. Xu, "A novel non-iterative inverse method for estimating boundary condition of the fur\ace inner wall," *Int. Comm. Heat Mass Transfer*, vol. 87, pp. 91–97, 2017. DOI: 10.1016/j.icheatmasstransfer.2017.06.017.

[24] B. Yu, C. Xu, W. Yao and Z. Meng, "Estimation of boundary condition on the furnace inner wall based on precise integration BEM without iteration," *Int. J. Heat Mass Transfer*, vol. 122, pp. 823–845, 2018. DOI: 10.1016/j.ijheatmasstransfer.2018.02.039.

[25] H. Zhou, Y. Li, B. Yu and H. L. Chen, "Shape identification for inverse geometry heat conduction problems by FEM without iteration," *Numer. Heat Transfer A Appl.*, vol. 72, no. 8, pp. 628–641, 2017. DOI: 10.1080/10407782.2017.1394128.

[26] B. Bin-Mohsin and D. Lesnic, "Determination of inner boundaries in modified Helmholtz inverse geometric problems using the method of fundamental solutions," *Math. Comput. Sim.*, vol. 82, no. 8, pp. 1445–1458, 2012. DOI: 10.1016/j.matcom.2012.02.002.

[27] M. Li, Z. Fua, W. Xu and C. Fan, "A novel spatial-temporal radial Trefftz collocation method for the backward heat conduction analysis with time-dependent source term," *Int. J. Heat Mass Transfer*, vol. 201, pp. 123627, 2023. DOI: 10.1016/j.ijheatmasstransfer.2022.123627.

[28] Q. Xi, Z. Fu, C. Alves and H. Ji, "A semi-analytical boundary collocation solver for the inverse Cauchy problems in heat conduction under 3D FGMs with heat source," *Numer. Heat Transfer B Fundam.*, vol. 76, no. 5, pp. 311–327, 2019. DOI: 10.1080/10407790.2019.1665386.

[29] Z. Fu, *et al.*, "Singular boundary method: a review and computer implementation aspects," *Eng. Anal. Bound. Element.*, vol. 147, pp. 231–266, 2023. DOI: 10.1016/j.enganabound.2022.12.004.
[30] Y. Gu, W. Chen and Z. Fu, "Singular boundary method for inverse heat conduction problems in general anisotropic media," *Inverse. Probl. Sci. Eng.*, vol. 22, no. 6, pp. 889–909, 2014. DOI: 10.1080/17415977.2013.840300.
[31] H. Chen, B. Yu, H. Zhou and Z. Meng, "Improved cuckoo search algorithm for solving inverse geometry heat conduction problems," *Heat Transfer Eng.*, vol. 40, no. 3–4, pp. 362–374, 2019. DOI: 10.1080/01457632.2018.1429060.
[32] J. T. Katsikadelis, *The Boundary Element Method for Engineers and Scientists: Theory and Applications*. Amsterdam, Netherlands: Elsevier, 2016.
[33] C. A. Brebbia and J. Dominguez, *Boundary Elements, an Introductory Course*. New York, NY: McGraw-Hill, 1989,
[34] C. H. Huang and C. C. Tsai, "A transient inverse two-dimensional geometry problem in estimating time-dependent irregular boundary configurations," *Int. J. Heat Mass Transfer*, vol. 41, no. 12, pp. 1707–1718, 1998. DOI: 10.1016/s0017-9310(97)00266-4.
[35] C. H. Huang and C. C. Tsai, "An inverse heat conduction problem of estimating boundary fluxes in an irregular domain with conjugate gradient method," *Heat Mass Transfer*, vol. 34, no. 1, pp. 47–54, 1998. DOI: 10.1007/s002310050230.
[36] H. Chen and H. Zhou, "Identification of boundary conditions for non-Fourier heat conduction problems by differential transformation DRBEM and improved cuckoo search algorithm," *Numer. Heat Transfer B Fundam.*, vol. 74, no. 6, pp. 818–839, 2018. DOI: 10.1080/10407790.2019.1591859.
[37] H. Chen, B. Yu, H. Zhou and Z. Meng, "Identification of transient boundary conditions with improved cuckoo search algorithm and polynomial approximation," *Eng. Anal. Bound. Element.*, vol. 95, pp. 124–141, 2018. DOI: 10.1016/j.enganabound.2018.07.006.
[38] B. Yu, G. Cao, S. Ren, Y. Gong and C. Dong, "An isogeometric boundary element method for transient heat transfer problems in inhomogeneous materials and the non-iterative inversion of loads," *Appl. Therm. Eng.*, vol. 212, pp. 118600, 2022. DOI: 10.1016/j.applthermaleng.2022.118600.
[39] R. Yadav, C. Balaji and S. P. Venkateshan, "Inverse estimation of number and location of discrete heaters in radiant furnaces using artificial neural networks and genetic algorithm," *J. Quant. Spectrosc. Radiat. Transfer*, vol. 226, pp. 127–137, 2019. DOI: 10.1016/j.jqsrt.2018.12.031.
[40] C. H. Huang, C. C. Chiang and H. M. Chen, "Shape identification problem in estimating geometry of multiple cavities," *J. Thermophys. Heat Transfer*, vol. 12, no. 2, pp. 270–277, 1998. DOI: 10.2514/2.6331.
[41] Q. Nguyen and C. Y. Yang, "Design of a longitudinal cooling fin with minimum volume by a modified Newton–Raphson method," *Appl. Therm. Eng.*, vol. 98, pp. 169–178, 2016. DOI: 10.1016/j.applthermaleng.2015.12.035.
[42] R. Beltman, T. Jan and W. Ijzerman, "A least-squares method for the inverse reflector problem in arbitrary orthogonal coordinates," *J. Comput. Phys.*, vol. 367, pp. 347–373, 2018. DOI: 10.1016/j.jcp.2018.04.041.
[43] H. Mohamed and L. Marcel, "Inverse method for simultaneously estimating multi-parameters of heat flux and of temperature-dependent thermal conductivities inside melting furnaces," *Appl. Therm. Eng.*, vol. 141, pp. 981–989, 2018. DOI: 10.1016/j.applthermaleng.2018.06.041.
[44] C. H. Huang and B. H. Chao, "An inverse geometry problem in identifying irregular boundary configurations," *Int. J. Heat Mass Transfer*, vol. 40, no. 9, pp. 2045–2053, 1997. DOI: 10.1016/s0017-9310(96)00280-3.
[45] J. Y. Tan and L. H. Liu, "Inverse geometry design of radiating enclosure filled with participating media using meshless method," *Numer. Heat Transfer A Appl.*, vol. 56, no. 2, pp. 132–152, 2009. DOI: 10.1080/10407780903107303.
[46] X. W. Gao and M. C. He, "A new inverse analysis approach for multi-region heat conduction BEM using complex-variable-differentiation method," *Eng. Anal. Bound. Element.*, vol. 29, no. 8, pp. 788–795, 2005. DOI: 10.1016/j.enganabound.2005.03.001.
[47] M. Cui, Y. Zhao, B. B. Xu and X. W. Gao, "A new approach for determining damping factors in Levenberg-Marquardt algorithm for solving an inverse heat conduction problem," *Int. J. Heat Mass Transf.*, vol. 107, pp. 747–754, 2017. DOI: 10.1016/j.ijheatmasstransfer.2016.11.101.
[48] B. Zhang, J. Mei, C. Zhang, M. Cui, X-w Gao and Y. Zhang, "A general method for predicting the bank thickness of a smelting furnace with phase change," *Appl. Therm. Eng.*, vol. 162, pp. 114219, 2019. DOI: 10.1016/j.applthermaleng.2019.114219.
[49] K. Yang, G. H. Jiang, H. F. Peng and X. W. Gao, "A new modified Levenberg-Marquardt algorithm for identifying the temperature-dependent conductivity of solids based on the radial integration boundary element method," *Int. J. Heat Mass Transfer*, vol. 144, pp. 118615, 2019. DOI: 10.1016/j.ijheatmasstransfer.2019.118615.

[50] W. W. Jiang, G. H. Jiang, C. H. Tan, K. Yang and X. W. Gao, "A new method for identifying temperature-dependent thermal conductivity in transient heat conduction problems based on element differential method," *Eng. Anal. Bound. Element.*, vol. 137, pp. 65–77, 2022. DOI: 10.1016/j.enganabound.2022.01.020.

[51] P. W. Partridge, C. A. Brebbia and L. C. Wrobel, *The Dual Reciprocity Boundary Element Method*. Amsterdam, Netherlands: Elsevier, 1992.

[52] L. C. Wrobel and C. A. Brebbia, "The dual reciprocity boundary element formulation for nonlinear diffusion problems," *Comp. Meth. App. Mech. Eng.*, vol. 65, no. 2, pp. 147–164, 1987. DOI: 10.1016/0045-7825(87)90010-7.

[53] K. M. Singh and M. S. Kalra, "Time integration in the dual reciprocity boundary analysis of transient diffusion," *Eng. Anal. Bound. Element.*, vol. 18, no. 2, pp. 73–102, 1996. DOI: 10.1016/S0955-7997(96)00014-8.

[54] L. C. Wrobel and C. A. Brebbia, *Boundary Element Methods in Heat Transfer*. Amsterdam, Netherlands: Elsevier, 1992.

[55] J. N. Lyness and C. B. Moler, "Numerical differentiation of analytic functions," *SIAM J. Numer. Anal.*, vol. 4, no. 2, pp. 202–210, 1967. DOI: 10.2307/2949389.

[56] J. M. Amado, M. J. Tobar, A. Ramil and A. Yáñez, "Application of the Laplace transform dual reciprocity boundary element method in the modelling of laser heat treatments," *Eng. Anal. Bound. Element.*, vol. 29, no. 2, pp. 126–135, 2005. DOI: 10.1016/j.enganabound.2004.12.005.